



Egyptian Knowledge Bank



***International Journal of Advances in Structural
and Geotechnical Engineering***

<https://asge.journals.ekb.eg/>

Print ISSN 2785-9509

Online ISSN 2812-5142

Special Issue for ICASGE'19

***FLEXURAL RESPONSE AND MOMENT
REDISTRIBUTION OF RC CONTINUOUS T-
BEAMS STRENGTHENED WITH FRP OR STEEL
BARS***

Tarek A. A. Khaled, Hesham M. A. Diab and Mohamed M. M. Rashwan

ASGE Vol. 03 (04), pp. 74-90, 2019

Flexural Response and Moment Redistribution of RC Continuous T-Beams Strengthened With FRP or Steel Bars

Tarek A. A. Khaled¹, Hesham M. A. Diab² and Mohamed M. M. Rashwan³

¹assistant lecturer, E-mail: tarek_gt@ymail.com

²Associate Professor, E-mail: heshamdiab2@yahoo.com

³Professor, Faculty of Engineering, Assiut University, Egypt

ABSTRACT

This paper is an experimental study to investigate the behavior of the RC continuous T-beams strengthened with NSM CFRP or steel bars under static loads. The experimental program consists of five RC continuous T-beams with overall dimensions equal to (200*300*4300) mm and with constant load (120kN) at the central loaded column. The first one was unstrengthened control beam designed to fail in flexure. Two beams were strengthened at the hogging region by using CFRP or steel bars, the other beams were strengthened at the mid-span region. The effect of strengthening material type and region on the load carrying capacity of the beams, deformation, ductility index and moment redistribution were investigated. Test results revealed that, three failure modes of beams were observed, namely the steel yielding, crushing of the concrete after steel yielding, end anchorage separation before the steel yielding at the strengthening region. The ductility of all strengthened beams was reduced compared with that of the respective unstrengthened control beam. The moment redistribution ratio depends deeply on the internal force at the main sagging reinforcement.

Keywords: Continuous beams, NSM bars, CFRP bars, strengthening, Serviceability.

INTRODUCTION

Many in-service civil and industrial buildings, bridge, municipal work, and hydraulic engineering may be repaired or rehabilitated due to materials decay, environmental corrosion, fire hazard, earthquake, impaction, structural function change, etc. It should be used in a safe, reasonable, economic the technology for strengthening and rehabilitated the structure rather than a simple and rough method. A new strengthening technique for reinforced concrete structures based on FRP or steel bars has been recently emerging as a valid substitute for traditional strengthening methods and externally bonded FRP sheets [1-3], NSM bars have been applied to strengthen RC structures for increasing the bearing capacity. Its use has several advantages over the externally bonded (EB) FRP technique: protection, improved bond, better aesthetics, and surface preparation, as described elsewhere [4, 5]. In the case where the failure of strengthened members is due to the NSM system failure, two different types of rupture are possible, the failure is due to the pull-out of the rods inducing almost splitting of the resin and concrete surrounding the groove or the peeling-off of the concrete covering the groove from the end of the rod [6].

Although many in situ RC beams are of continuous construction, there has been very little research into the behaviour of such beams [7-11]. However, moment redistribution in such elements was reported in previous studies [12-19]. The observed moment redistribution was attributed to the relatively low modulus of elasticity of the FRP bars, compared to that of steel bars, the plasticity of concrete at high-load levels and the different bond characteristics of the FRP bars, in addition to the difference in the flexural stiffness between the critical sections. In these studies, parameters such as material type, reinforcement ratio and configuration, concrete

strength, stirrup spacing in the context of beams with rectangular and T-section were investigated. As described, the majority of the research investigated the strengthening of RC continuous beams with external bonded sheet or studied the fiber reinforced polymer-reinforced concrete continuous beams without central column, and sometimes, there will be no ability to strength the reinforced concrete continuous beams at the different maximum moment regions together. In this study, the main objective is to investigate the behavior and moment redistribution of large-scale RC continuous T-beams subjected to static loads. The serviceability and moment redistribution of continuous concrete specimens strengthened with NSM bars at the negative moment or at the positive moment region with different material are studied and compared with unstrengthened beam.

Beams and strengthening technique

Beams

The test specimens consisted of Five RC continuous beams as given in Table1. All tested beams were RC continuous beam with length 4300 mm and, the T-cross section dimensions were 200 * 230 mm and 400*70 mm for the web and the flange respectively. Tested beams had a central loaded column with dimensions 200*200 mm and total length was 700mm. The main reinforcement was two high tensile steel bars of (12) mm diameter on the flange of the beam and two high tensile steel bars of 16 mm diameter on the positive moment region. All columns reinforced with four bars 12 mm as a longitudinal reinforcement and 8 mm transverse reinforcement at intervals of 100 mm. By prestressing a 25 mm deformed bar, the central columns were loaded by about 120 kN as a constant load before loading the beams (Fig. 1).

The tested beams including a control beam (CB) and four strengthened beams (SSH, SCH, SSS and SCS) with NSM bars of limited bond length 1500 mm at the hogging or the sagging region. Table 1 isolates them and shows their characteristics. Two of them (SSH and SSS) were each strengthened with one NSM steel bars at the hogging and the sagging regions, respectively. The tested beam (SSH) strengthened with two steel bars (2D12) and the tested beam (SSS) strengthened with one steel bar (2D16). Two more beams (SCH and SCS) each strengthened with NSM FRP bars at the hogging and the sagging regions respectively. All strengthening beams were designed to have a similar load-carrying capacity of approximately ($p=210$) kN, where (p =applied load at the middle of each span). A special concrete saw was used to cut the grooves at the surface of the beam. The square groove dimension was 25 mm. The epoxy was pressure added into the grooves to cover of the groove height, the bars were located in the grooves and gradually pressed to dislocate the bonding agent as shown in Fig. 2. The grooves were then filled totally with the epoxy. Two steel anchors were bonded to the ends of the CFRP and steel bars with epoxy, these anchors had a rectangular shape with dimensions 100*300 mm and 100*150 mm for the beams which strengthened at the hogging and the sagging respectively, and with 4 mm thickness, as shown in Fig. 2.

To strengthening the continuous beams at the existing building, there is no clear difference with the laboratory preparation, but it shall be

Table 1. Compressive strength, reinforcement for the tested beams and strengthening method:

Beam	f_{cu} (MPa)	Length m	Steel shear stirrups	Bottom RFT.	Top RFT.	Strengthening method	
						region	Material type
CB	27.5	4.30	Φ8/100 mm	2Φ16	2Φ12	—	—
SSH	35.5					Hogging	Steel (2Φ12)
SCH	33					Hogging	CFRP (2Φ12)
SSS	34					Sagging	Steel (1Φ16)
SCS	34					Sagging	CFRP (1Φ12)

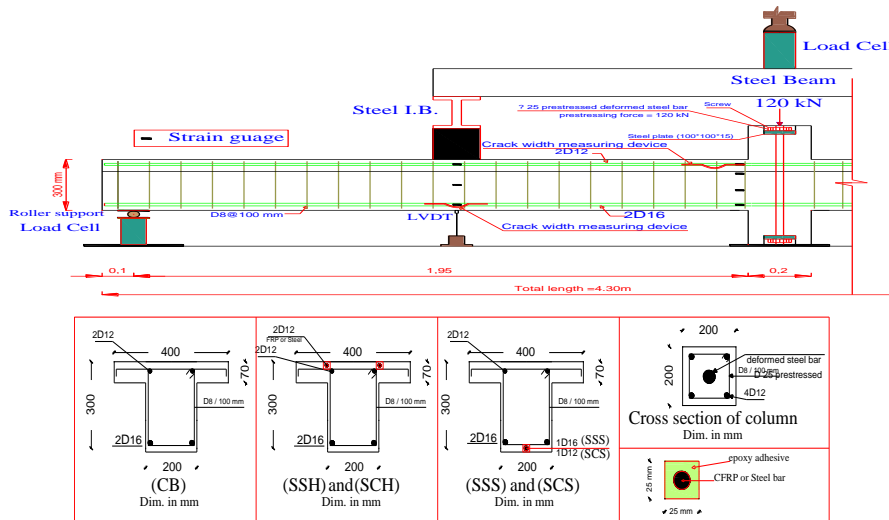


Fig. 1. Details of reinforcement, typical cross-section, strengthening method and test set up instrumentations for the tested beams.



Fig. 2. Shape of the grooves and steel anchors for the strengthened beams with NSM bars.

Material properties

All beams were made of typical concrete, the concrete required a mix proportion of 1:1.7:3.0 (Cement: Sand: Coarse aggregate) by weight of cement, and coarse aggregates of a maximum nominal size of 10 mm. The water–cement ratio was 0.45 and the designed 28-day cube compressive strength of concrete was 30 MPa. The compressive strength f_{cu} of the concrete obtained for each beam from compression tests carried out on three 150 mm cubes at test day is given in Table 1.

High tensile steel used for the longitudinal reinforcement and mild steel for shear reinforcement (stirrups), the mechanical properties of the reinforcing bars used in this study shows in Table 2.

Sika CarboDur BC Rods and epoxy adhesive Sikadur-30 LP were used to prepare the CFRP composite material. The mean value of the tensile strength, the elasticity modulus and the ultimate strain in longitudinal direction of fibres of each bar of the carbon fiber given by manufacturer were 3100 MPa, 148 GPa and 1.70%, respectively. Epoxy resin has been a tensile strength of 42 MPa, the elasticity modulus of 10 GPa and ultimate strain of 1.5%. Epoxy adhesive Sikadur-30 LP was also used for NSM steel bars.

Bar size	Bar diameter (mm)	Bar Area (mm^2)	Modulus of elasticity (GPa)	Yield Strength (MPa)	Yield strain ($\mu\epsilon$)	Tensile Strength (MPa)	Ultimate strain ($\mu\epsilon$)
8	7.6	45.36	200	360	2800	482	72820
10	10	78.5	196	509	3010	665.80	65000
12	12	113	210	522	3280	640.60	58543
16	15.95	199.81	203	542	3680	637.81	45180

Table 2. Mechanical Properties of the Reinforcing Bars:

Instrumentation and Test Setup

For the all tested beams, the central support was the loaded column, so the two load cells were used at the end supports. Also, for all beams, the LVDTs were used under point load in the middle of each span to measure the deflections as shown in Fig. 1. Additionally, crack width gauges were installed in the middle of each span to record the crack width at the sagging region. For the hogging region, there were two Crack width gauges were installed at the flange next to the column. Regarding electrical strain gauges for the control beams (CB), they consisted of six electrical strain gauges for longitudinal reinforcement, for the hogging region (one strain gauge for ϕ 12) at the critical section. For sagging region (one strain gauge at the main steel reinforcement and other at the compression steel at the critical section at every span). Plus, two concrete electrical strain gauges were used at the hogging critical section to observe the neutral axis depth at every stage of loading, and one concrete electrical strain gauge was used at the sagging critical section for the same reason. The electrical strain gauges in the strengthened beams, they had the same electrical strain gauges like the control beam (CB), and there were two electrical strain gauges for the strengthening bars at the critical sections on the sagging or the hogging regions.

Experimental results and discussion:

A 5,000-kN hydraulic machine was used to apply concentrated load on a stiff steel beam that in turn transmitted the load to the midpoint of each span. The load applied on each span was then evenly transferred to the beam by the associated steel beam as shown in Fig. 3. Loading was applied at a rate of 15 kN/min. Readings of all instrumentations were acquired and stored using a data logger (TDS 150) system monitored by a computer. The obtained experimental results are presented and discussed subsequently in terms of the observed mode of failure, crack width, load–deflection response, ductility analysis, load carrying capacity, flexural rigidity, energy absorption, strain in reinforcement and moment redistribution.



Fig. 3. System of loading on beams.

General behavior:

For the control beam (CB), the first cracks appeared at loads 76.88 and 53.80 at the hogging and the sagging regions respectively. The hogging longitudinal reinforcement was yielded at

load 260kN followed by yielding of the sagging longitudinal reinforcement at load 278.03 kN. While the concrete crushing was at 347.22 kN. The deflection values at the yield loads for the hogging and the sagging regions were 7.83mm and 10.97 mm respectively, while at ultimate load it was 51.07 mm. The big difference between the deflection values at the yield loads and the ultimate load illustrates the good ductility of the CB. For the other beams, the cracking loads range between (70kN: 85kN) for the sagging region and (76kN: 101kN) for the hogging region. As they are close values with the cracking loads for the control beam, and there were not a clear difference between the strengthening beams at the values of the cracking loads, where the cracking load depends mainly on the concrete compressive strength and the gross moment of inertia for the tested beams. Strengthening the continuous RC beams at the sagging or the hogging region led to increase in the yield load by about 52% for the beam SSH at the negative moment region and by about 33% for the beam SCS at the mid-span region. The ultimate load for all strengthening beams increased by acceptable value which ranged between (10%: 25%) compared to the control beam (CB). The strengthening beams failed by steel yielding in the unstrengthened region followed by separation of the plate end, as shown in Fig 4. The crack width for the strengthening beams was less than that of the control beam at all loading stages. Where the crack width at the bottom region for the CB was 11 mm at the failure load, but it ranged between 1.7mm and 8.3mm for the others. Fig. 4 shows the mode of failure for all tested beams.

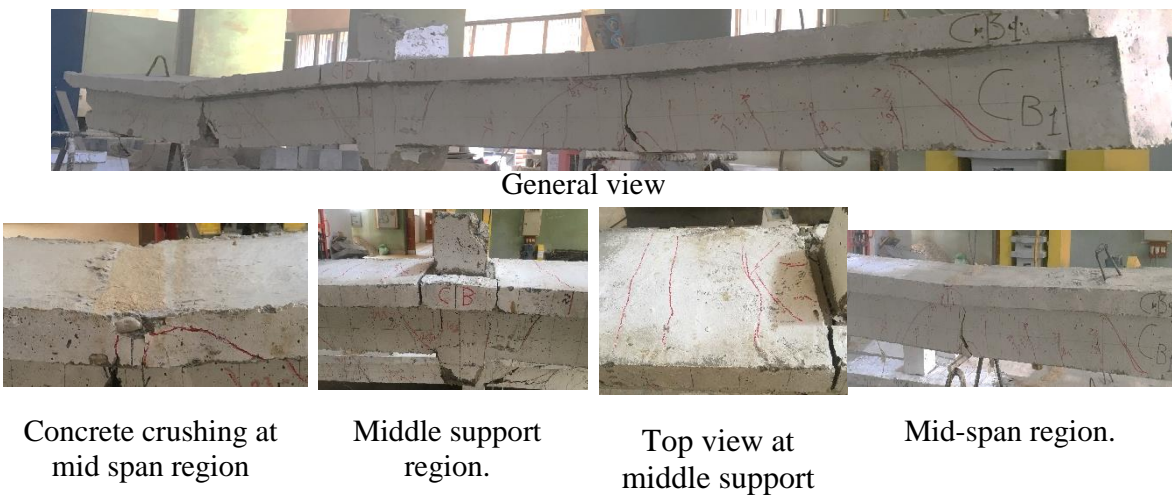


Fig.4.a. Failure modes of beam CB.

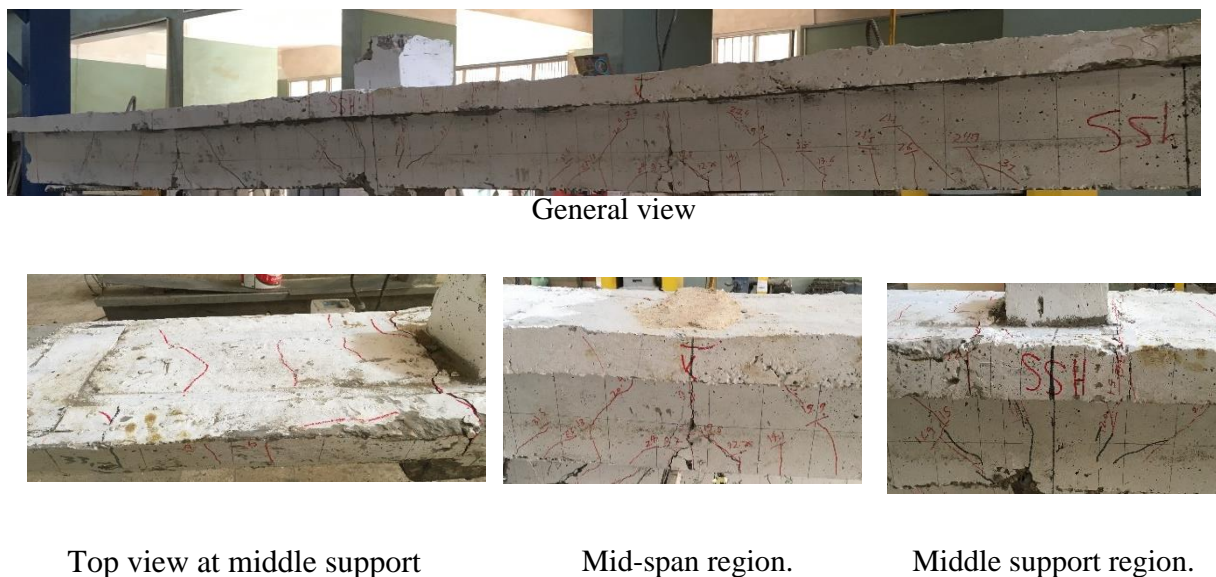


Fig.4.b. Failure modes of beam SSH.



General view



separation at the plate end.



Middle support region.



Top view at middle support



Mid-span region.

Fig.4.c. Failure modes of beam SCH.



General view



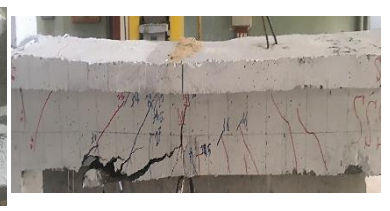
separation at the plate end.



Middle support region.



Top view at middle support



Mid-span region.

Fig.4.d. Failure modes of beam SSS.



General view

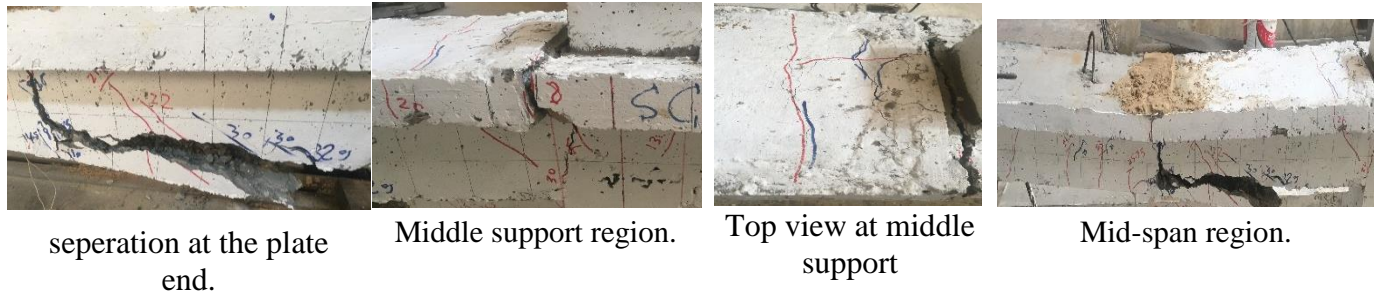


Fig.4.e. Failure modes of beam SCS.

Effect of the strengthening material type: Strengthening the hogging region:

The load-deflection response for the control beam (CB) and the strengthening beams (SSH and SCH) can be clearly seen in Fig. 5. From Fig. 5, it can be observed a correlation in load-deflection curves until the cracking loads with linear load-deflection behavior. After the cracking loads, the flexural stiffness gradually reduced in all beams but the value of the deflection quickly increased at the unstrengthened beam (CB), beginning from the yield load the load-deflection curve started to be horizontal until the failure load. At the strengthened beams (SSH and SCH), the slope of the curve is higher, especially for the strengthened beam (SCH), where the slope of the curve is slightly reduced to failure. The strengthened beam (SSH) gave a deflection value more than the strengthened beam (SCH), this high deflection value of the NSM-steel strengthened beam is a big advantage as it shows much more ductile behaviour. This gives an ample warning before failure which is similar to the steel reinforced beam.

Fig. 6 (a and b) shows the relationship between the total load and the tensile strains of the main longitudinal reinforcement at the hogging and the sagging regions respectively. As shown, the failure of the control beam (CB) occurred as a result of the steel yielding where the main top reinforcement yielded at load 260 kN and then followed with yielding the sagging longitudinal reinforcement at load 278 kN. The strain at the sagging region was equal to 1.89 times of the yield steel strain at the failure load, while the max tensile steel strain at the negative moment region was equal to 2.82 times of the yield steel strain. It can be clearly observed that the strengthening at the hogging region with NSM bars affected on the strains of the main steel reinforcement, either in the hogging or the sagging region, especially in the case of using NSM steel bars. The maximum tensile strains at the mid-span region for beams (SSH) and (SCH) were equal to 9.45 and 9 times of the yield steel strain respectively, and approximately 5 and 4.8 times of the control beam steel strain at failure. For the maximum steel strain at the middle support section, for beam SSH, were equal to 6.1 and 2.15 times of the yield steel strain and maximum strain at the control beam respectively. While the beam SCH had a maximum tensile strain equal to 1.6 times of the yield steel strain and 0.57 of the control beam maximum strain. Therefore, using the NSM CFRP bars led to a sudden failure due to the separation at the plate end, but in the case of using the NSM steel bars increased the deformation and thus gave a warning before the failure. The strain at the NSM steel bars for beam SSH was $46474.74 \mu\epsilon$, which was equal to 14.52 times of the yield steel strain. At the beam (SCH), the NSM CFRP bars strain was $5450 \mu\epsilon$, and it was 0.32 times of the ultimate CFRP bars strain.

Strengthening the sagging region:

The effect of the type of NSM bars used at the sagging region can be clearly seen in Fig. 7. As for the strengthening at the hogging region, the load-deflection curves are almost identical until after the cracking loads. However, it can be noticed that, the flexural stiffness for the strengthening beams (SSS and SCS) is significantly higher than the control beam (CB) even reach the ultimate load and yield load for beams (SSS and SCS) respectively. The mid-span deflection values for the beams (SSS and SCS) are approximately equal even though the beam (SSS) which strengthened with NSM steel bar, was expected to have higher mid-span deflection value, but the similarity due to a sudden failure. The sudden drop at the load-deflection diagram

(Fig.7) is due to the flexural shear cracks between the load point and the column which led to separation of the plate suddenly.

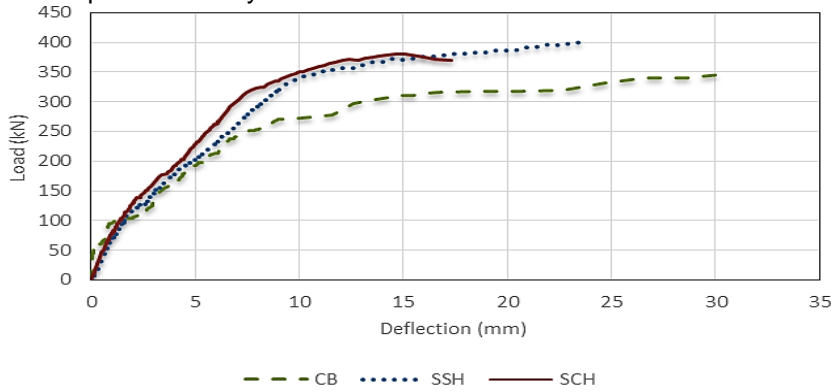


Fig.5. load-deflection relationship for the tested beams (CB, SSH and SCH).

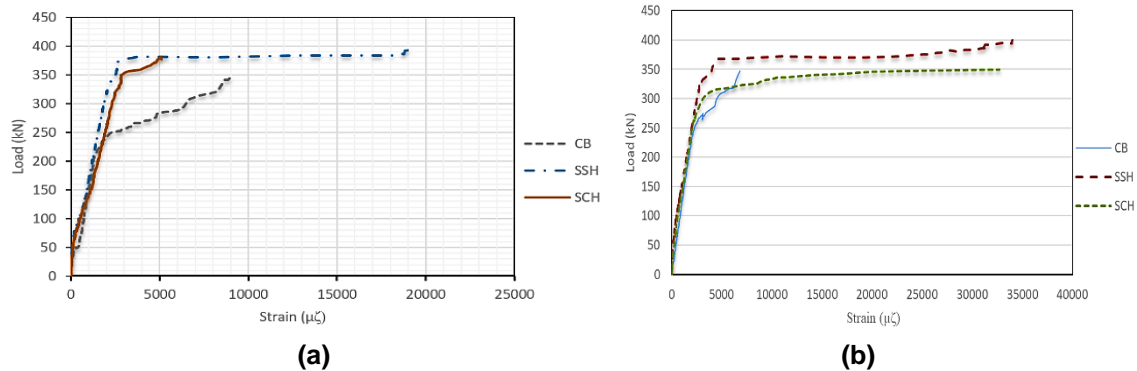


Fig. 6. Load-micro strain relationship at the top and bottom reinforcement for beams (CB, SSH and SCH).

Fig 8 (a and b) shows the relation between load and strains in the tension strain at the hogging and the sagging regions for the tested beams (CB, SSS and SCS). Load-strain behavior for the main top and bottom longitudinal reinforcement was linear until cracking. From Fig. 10 for the critical sections at the hogging region, it is obvious that the flexural stiffness of the strengthening beams was rapidly reduced compared to the control beam (CB), but the curves continued linear at a lower slope up to yield of the hogging tension steel, after which the curves were nonlinear up to failure. It is also noticeable that the ultimate tensile strain for the strengthening beam converge at failure with the maximum strain value of the control beam, where these strains were 9050, 9901 and 10600 $\mu\epsilon$ for beams (CB, SSS and SCS) respectively. For the tension strains at the sagging region, the ultimate tension strains of the strengthening beams (SSS and SCS) were equal to 1.31 and 0.88 times of the maximum strain of the control beam, and about 2.47 and 1.67 times of the yield steel strain respectively. The curves also show that the strengthening at the sagging region with NSM steel provided an increase in the flexural rigidity from the beginning of the loading compared to the control beam and beam (SCS), and it improved the ductility despite the sudden failure. The maximum tension strains for the NSM bars were 11584 and 6795 $\mu\epsilon$ for beams (SSS and SCS) respectively, these strains are equal to the 3.22 times of the yield steel strain for beam (SSS) and 0.4 times of the ultimate CFRP strain for beam (SCS), this value was higher than that which in beam SCH.

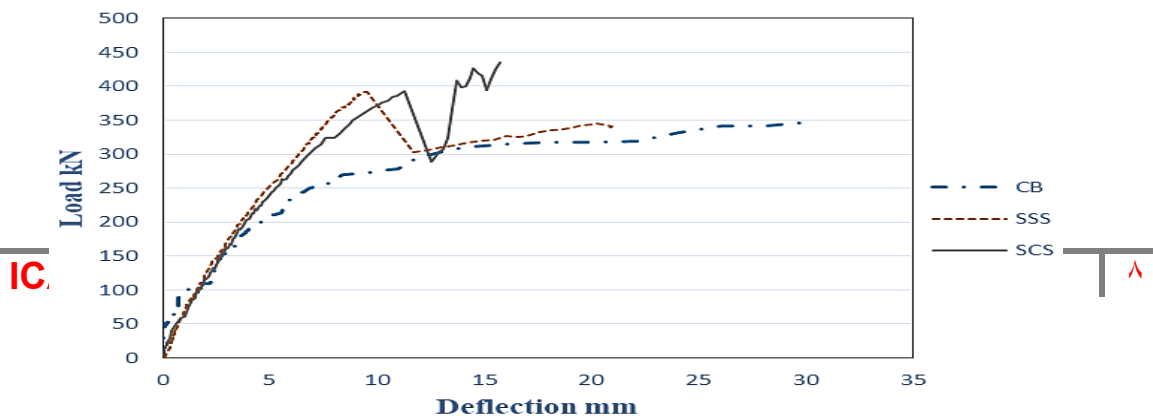


Fig.7. load-deflection relationship for the tested beams (CB, SSS and SCS).

Beam	Δ_{yh} mm	Δ_{ys} mm	Δ_u mm	Δ_f mm	$\mu_{\Delta u}$	$\mu_{\Delta f}$
CB	7.83	10.97	33.1	33.1	4.23	4.23
SSH	17.23	9.9	23.55	23.55	2.38	2.38

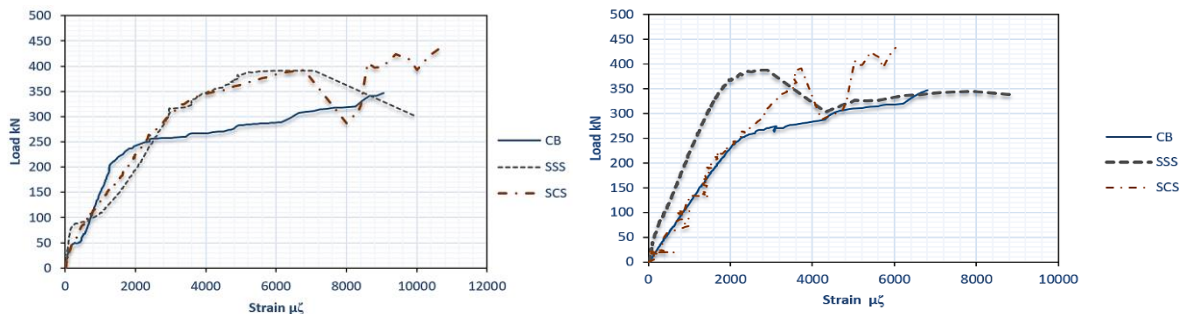
(a)

(b)

Fig. 8. Load-

crack width relationship at the sagging region for all tested beams.

Ductility analysis



Ductility is a desirable structural property that allows stress redistribution and provides working of impending failure. Ductility can be defined as the ability of the structure to undergo inelastic deformations at near maximum load without brittle failure. This deformability is influenced by some factors such as the level of axial load, the shape of the section, the amount of transverse reinforcement, the tensile reinforcement ratio, the compressive reinforcement ratio, the yield strength of reinforcement and the strength of concrete.

The displacement ductility index is expressed in this study as follows [20, 21].

$$\mu_{\Delta u} = \Delta_u / \Delta_y \tag{1}$$

$$\mu_{\Delta f} = \Delta_f / \Delta_y \tag{2}$$

Where Δ_u and Δ_f is the midspan deflection at the beam ultimate load and failure load, Δ_{yh} and Δ_{ys} is the midspan deflection at the yielding load of the tensile steel reinforcement at the central support and the midspan respectively, μ_u and μ_f is the displacement ductility index at ultimate load (maximum load carrying capacity) and at failure load. Δ_y , that was used to calculate the displacement ductility, in which the curves changed from linear to nonlinear. The displacement ductility index (μ_{Δ}) is given in Table 3.

From Table 5, It was observed that the ductility of the beam specimens was adversely affected by the strengthening, whether it was strengthened with NSM CFRP or steel bars. But for the beams (SSS and SCS), which were strengthened at the sagging region, their ductility continued to increase after the ultimate load in contrast to the beams (SSH and SCH), where the sagging main tensile steel did not yield at the end cover separation load, therefore there was a reload of the beam. In general, it was noted that the strengthening with NSM steel bars worked on increasing the ductility of the tested beams, where the displacement ductility index for the beam SSH was higher than the beam SCH by about (15%), and the displacement ductility index at the failure load for the beam SSS was higher than the beam SCS by about (15%).

Table 3 Summary of ductility index:

SCH	10.66	7.29	15.1	15.1	2.07	2.07
SSS	6.88	8.13	9.52	20.71	1.14	2.55
SCS	7.8	7.09	11.13	15.7	1.57	2.21

Enhancement of the load carrying capacities and the Serviceability state

Fig.9 presents the yield, ultimate and failure loads carrying capacities for the all tested beams. As shown in Fig. 9, the yield load for the top and bottom main reinforcement and the ultimate load for the control beam (CB) were 260, 278 and 347 kN, as previously explained, the sagging tensile reinforcement yielded after the yielding of the hogging main reinforcement and before the maximum load. The yield loads at the hogging and the sagging region were equal to (75% and 80%) of the ultimate load.

The yield loads were affected by the region of the strengthening, where unlike the others, the main top reinforcement at the strengthening beams (SSH and SCH) yielded after the mid-span tensile steel yielding, thus, there was a clear variation in the values of the yielding loads, but the yield loads for all strengthening beams were higher than the yield loads of the control beams. The strengthened beam (SCH) had the less sagging yield load between the strengthening beams and it was higher than the sagging yield load of the control beam by about (11.5)%, while the minimum hogging yield load was for the strengthened beam (SSS) and it increased by about (22.7)%.

Despite the convergence of the failure loads values, but the strengthening by using NSM CFRP bars at the sagging region was higher than the failure load at the control beam by (25%) and it was the best efficiency, even though the least efficient was for the strengthening at the hogging region by using NSM CFRP bars, where the maximum load increased only by (10 %).

Unlike simply supported beams, the enhancement of the bending moment capacity of a continuous beam due to strengthening with NSM bars was found to be higher than that of the enhancement of the load capacity. The beams (SSH and SCH) exhibited an increase in the in the negative moment by about (61.5% and 40%) respectively. For the strengthening at mid-span region, there was an increase in the positive moment by about (24 %) at the ultimate load for the beam (SSS) and (32.7%, 47.7%) for the beam SCS at the first separation and the ultimate load, respectively.

Serviceability is a basic characteristic of comparison, the serviceability of the tested beams can be determined according to [20, 21] by using permissible crack width, allowable permitted deflection, and allowable yield strain, Table 6 shows the measurement value of the load at hogging and sagging regions for different levels of flexural crack width (0.1, 0.2, 0.3). The flexural crack width " w_{cr} " (0.1, 0.2 and 0.3 mm) is the permissible crack width according to [20, 21]. It is clear that strengthening with NSM CFRP bars gave preference for the load at the same crack width at the strengthening region only, but the strengthening by using NSM steel bars had the advantage at both regions, although the service load was fewer at the strengthening region than using NSM CFRP bars.

The maximum deflection should be compared to the allowable permitted deflections in codes and design guidelines. The allowable deflection permitted by [20, 21] ranges from L/480 to L/180 depending on the type and function of the structure. The allowable deflection for tested beams according to [2 and 3] should be within the range of 4–11 mm (2,050/480 to 2,050/180) based on the type of structural application. So according to the structural type, the strengthening at the sagging region by NSM steel or CFRP bars was better than other types of strengthening in the case of The allowable deflection equals L/180 and L/480, and the strengthening by using NSM steel bars was better than the others where the allowable deflection was after the ultimate load. As shown in Table 4.

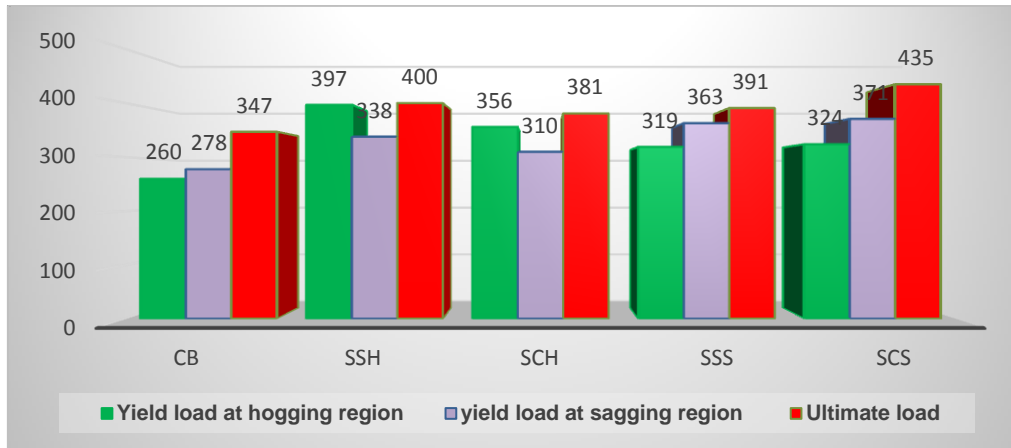


Fig. 9. Load carrying capacities for all tested beams.

Table 4. Load carrying capacities at different serviceability limits:

Beam	w_{cr} (mm)	P_1 (kN)		P_2 (kN)	
		Hogging region	Sagging region	at $l/480$	at $l/180$
SSH	0.2	145	109	187	354
	0.3	172	124		
	0.1	118	101		
SCH	0.2	250	132	200	362
	0.3	347	158		
	0.1	263	76		
SSS	0.2	333	101	227	302*
	0.3	380	154		
	0.1	124	108		
SCS	0.2	173	147	213	393
	0.3	286	192		
	0.1	114	74		
	0.2	268	108		
	0.3	324	142		

P_1 : The load at the hogging or the sagging region for the permissible crack width.

P_2 : The load at the allowable deflection.

(*) After the ultimate load (where $P_u = 391$ kN).

Moment redistribution

The moment redistribution ratio (β) given in Table 6 was calculated for the sagging and the hogging bending moment at midspan and at the central support at any stage of the loading. The ratio was calculated by (3):

$$\beta = \frac{M_e - M_{ex}}{M_e} * 100 \quad (3)$$

Where M_e , is the value of the moment at central support and mid-span is based on the elastic analysis and M_{ex} is the experimental value of bending moment at any stage of loading.

- From Fig. 10 (a and b) and Table 5, it can be seen that the redistribution of the internal force from the sagging to the hogging region gradually decreased at the beginning of the test until the cracking load for the control beam, CB, where the moment redistribution ratio was almost equal to zero. After the cracking load and before reaching the steel yielding ($P_y = 278$ kN), the moment redistribution ratio increased with a slow rate where the maximum moment redistribution ratio was -9.9% and 14.76% at the sagging and the hogging regions, respectively. The moment redistribution reduced after the steel yielding and this could be attributed to the reduced flexural stiffness due to the extensive cracking observed in the higher load span. Regarding the effect of the strengthening region, both beams SSH and SCH redistributed moments in a similar manner up to failure. The difference in the strengthening at the hogging region was that the internal forces redistributed from the sagging to the hogging moment region up to failure because the NSM bars was able to control the crack widths which in turn, made the middle support region stiffer than the sagging moment region. Although the moment redistribution ratio decreased due to the convergence of the flexural rigidity between the mid-span region and the central support region, this ratio increased again after the yielding of the sagging steel and up to failure as a result of the increase in the cracks width at the sagging region. The moment redistribution ratio for the beam (SSH) at the steel yielding was 11.5% and -15.56% at the sagging and the hogging region respectively, and then the rapid increase until failure, especially for the negative moment. The moment redistribution ratio at the failure was 16.15% and -23.43%. For the strengthened beam (SCH), the moment redistribution ratio significantly reduced and this value was roughly equal to zero at steel yielding. Where the percentage reduced to 0.5% and -0.8% at the sagging and the central support region respectively, because the axial stiffness of the upper main reinforcement with the NSM bars was slightly higher than the axial stiffness of the bottom main reinforcement. Close to failure, beam SCH achieved 10.12% and -16.7% moment redistribution at the mid-span and the hogging region, respectively. Beams SSS and SCS demonstrated load redistribution from the middle support to the mid-span section such as the control beam. This is due to the stiffness at the mid-span section was 2.66 and 2.17 times of the hogging section for beam SSS and SCS, respectively. As it was indicated in the other beams, the deviation in the load-moment redistribution ratio curve was at the sagging steel yielding. The beam SSS achieved -21.28% and 35.93% moment redistribution at the sagging and the hogging region before the steel yielding, while these percentage reduced at the failure to -16.4% and 27.33%. The maximum value for the moment redistribution ratio was achieved by the beam SCS, the percentages of moment redistribution were -25.2% and 42% at the sagging and the middle support, respectively. About the approximate formula to calculate the contribution of the method of repair or strengthening as to the moment redistribution of the beam, this paper is the first edition and there will be other research about this point.

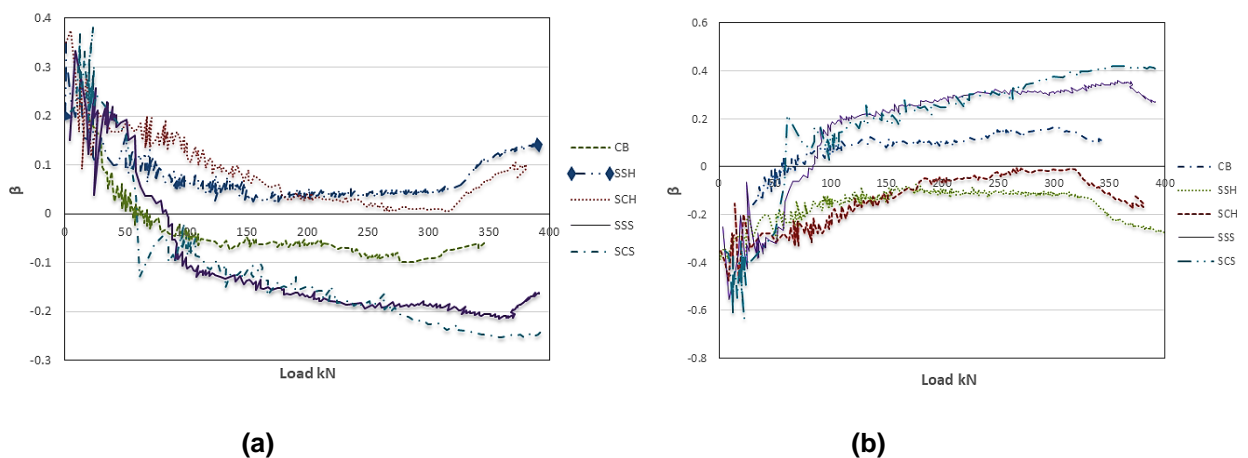
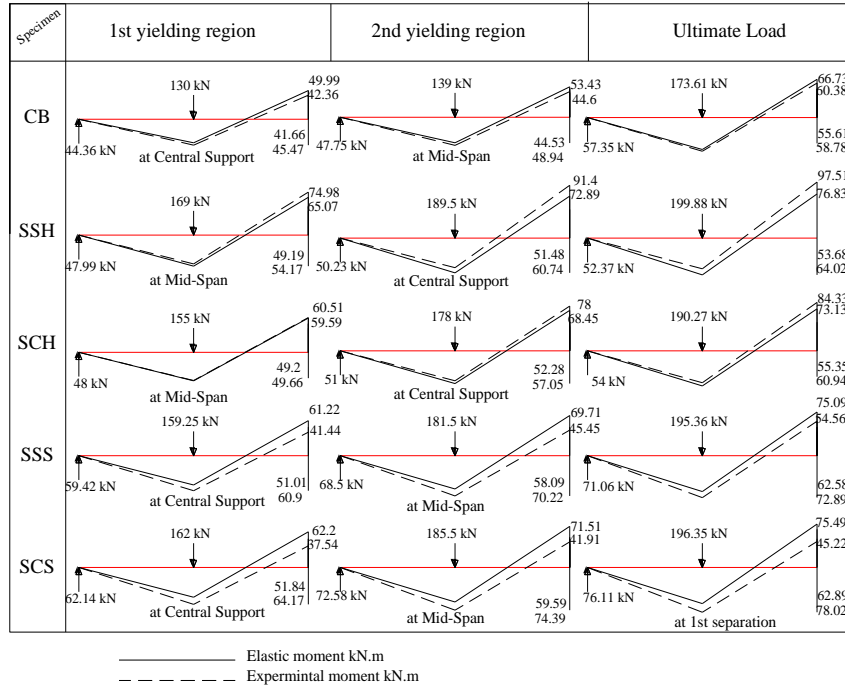


Fig.10. Load-moment redistribution ratio at the sagging region for all tested beams.

Table 5 End support reaction, moments at yield, ultimate loads and moment redistribution of the tested beams.



The prediction of ultimate load

The ultimate load of the strengthened beams is assessed by the force equilibrium and strain correlation requirements [22], as presented in Fig. 11 and 12. Failure of the strengthened beam is anticipated as the crushing of the compression concrete after yielding of the tension reinforcement. The computation is executed in the constant moment zone.

At failure, the forces C , T_s and T_{NSM} are shown in the following expression (Fig. 11 and 12):

$$C = 0.67 b a f_{cu} \tag{4}$$

$$T_s = A_s F_y \tag{5}$$

$$T_{NSM} = A_{NSM} E_{NSM} \epsilon_{NSM} \tag{6}$$

$$\epsilon_{NSM} \text{ is calculated by } \epsilon_{NSM} = \epsilon_c \frac{d_{NSM} - a}{a} \leq k_m \epsilon_{NSMu} \tag{7}$$

This value is taken from manufacturer. For the FRP bars used in this study, the k_m value was taken as 0.7.

For the NSM FRP bars $\epsilon_{NSM} = \frac{f_{NSM}}{E_{NSM}} \tag{8}$

The balance of forces produces the subsequent relation:

$$0.67 b f_{cu} a^2 + (\epsilon_{NSM} E_{NSM} A_{NSM} - A_s F_y) a - \epsilon_c E_{NSM} A_{NSM} d_{NSM} = 0 \tag{9}$$

The depth of the neutral axis (a) is determined using the Eq. (9).

The ultimate bending moment computes the following relation:

$$M_u = A_s F_y \left(d_s - \frac{a}{2} \right) + E_{NSM} A_{NSM} \epsilon_c \left(\frac{d_{NSM} - a}{a} \right) \left(d_{NSM} - \frac{a}{2} \right) \tag{10}$$

Referring to ACI 440.1R-15 [23], an additional reduction factor of $\psi f = 0.85$ was applied to the flexural strength contribution of the FRP reinforcement. This reduction factor is meant to account for the lower reliability of the FRP reinforcement, as compared with internal steel reinforcement. If the factor is induced here, the nominal flexural strength of strengthened beams with NSM FRP bars under compression failure can be computed using Eq. (15).

$$M_u = A_s F_y \left(d_s - \frac{a}{2} \right) + \psi f E_{NSM} A_{NSM} \epsilon_c \left(\frac{d_{NSM} - a}{a} \right) \left(d_{NSM} - \frac{a}{2} \right) \tag{11}$$

Fig. 10 shows the elastic theory bending moment diagram assuming uniform flexural rigidity along the length of the tested specimens. In this figure, M_{se} and M_{he} refer to the elastic moments in the sagging and hogging regions, respectively; R_{ee} and R_{me} are the elastic reactions at the end and middle support, respectively; and P is the applied load at each span.

The prediction of the flexural capacity of the test specimens was based on satisfying equilibrium conditions and assuming that both the mid-span and central support sections have high ductility and reached their flexural capacities M_{us} and M_{uh} , respectively. Accordingly, from equilibrium considerations, the applied load P was calculated in accordance to the provisions of ACI 440.1R-15 [23] and ACI 318-14 [20], respectively. The applied point load, P at the beam mid-span is calculated from (beam self-weight is neglected) (Table 6):

$$P = \frac{2}{L}(M_{uh} + 2M_{us}) \tag{12}$$

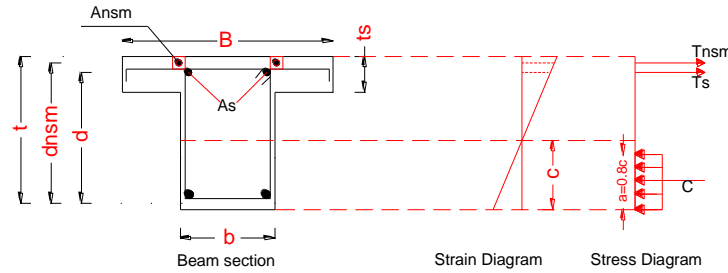


Fig. 11. Strengthened beam section with strain and stress distribution for the beams (SSH and SCH).

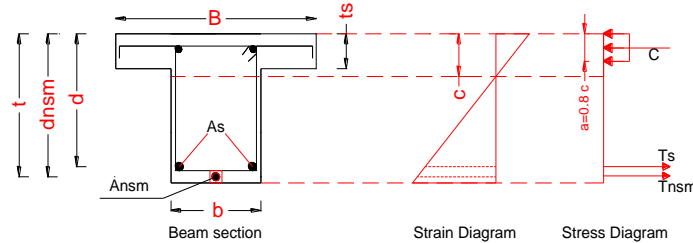


Fig. 12. Strengthened beam section with strain and stress distribution for the beams (SSS and SCS).

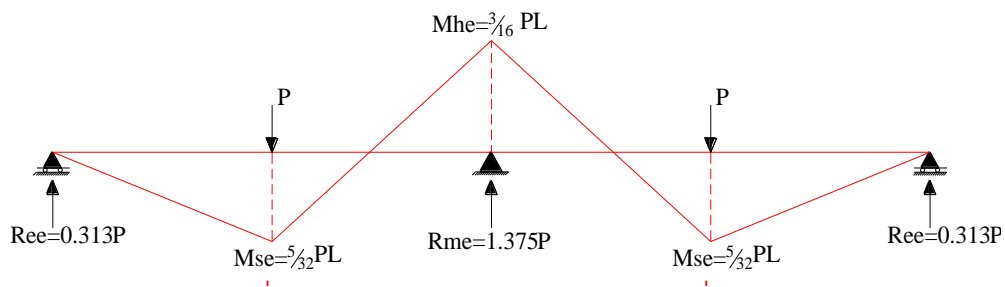


Fig. 13. Elastic Bending Diagram.

Table 6. Comparison between experimental and predicted results.

Specimen	Central Support		Mid-span		P_{exp}	P_e	Exp. /Pre.
	M_{exp} (kN m)	M_{pred} (kN m)	M_{exp} (kN m)	M_{pred} (kN m)			
CB	-60.38	-34.80	58.78	62.20	347.22	310.63	1.12
SSH	-97.51	-70.81	53.68	63.20	399.75	384.8	1.04
SCH	-84.33	-98.78	55.35	62.95	380.53	438.4	0.87

SSS	-54.56	-35.34	72.89	94.20	390.71	436.57	0.89
SCH	-45.22	-35.34	78.02	94.89	435.18	439.26	0.99

Conclusions

An experimental work was carried out on five large-scale RC continuous T-beams, to study the flexural strengthening of reinforced concrete continuous beams with central loaded column and by using near-surface mounted (NSM) CFRP or steel bars on the general behavior of the tested beams and their ability to redistribute bending moment between hogging and sagging regions under the influence of vertical loads. Based on the test results and the comparisons between the tested beams which presented in advance in this research the following conclusions can be drawn:

1. The first crack always formed in the sagging region for all tested beams as the main factor is the shape of the cross-section, also it wasn't affected by the strengthening region.
2. In general, strengthening by NSM reinforcement improved the overall flexural behavior of the beams at service and ultimate conditions, but also decreased the ductility of the beams when compared with the control beam.
3. The cracks concentrated at the maximum moment regions for beam CB, as a result of yielding the bottom reinforcing steel after the top reinforcing steel directly. In contrast, the strengthening beams, there was an increase in the number of the cracks and their spread along the beam span.
4. All strengthened beams failed after yielding of the tension steel reinforcement with separation of the plate end except the strengthening with the NSM steel bars at the negative moment .
5. Strengthening at the sagging region improves the ductility after the separation of the plate end, where the sagging main reinforcement didn't yield before the separation, unlike the strengthening at the hogging region.
6. Despite the premature failure, strengthening at the sagging region with CFRP bars had the maximum ultimate load value.
7. Unlike simply supported beams, the enhancement of the bending moment capacity of a continuous beam due to strengthening with NSM bars was found to be higher than that of the enhancement of the load capacity.
8. The stiffness of the beam strengthened at the hogging region is less than the beams strengthened at the sagging region, especially after yielding of the tensile steel.
9. The bottom reinforcement was the main controller in changing the values of moment distribution ratio, whether in the case of strengthening at the positive or negative region.
10. Hogging moment redistribution over the middle support is always larger than that at the mid-span by different values depending on the type and location of the strengthening.

Recommendations and suggestions

From the predescribed analysis of the test results and the above conclusion, it is recommended for the future research work the following topics:

1. Study the flexural response and moment redistribution of RC continuous T-beams strengthened with FRP or steel bars by using different anchor system.
2. Study the flexural response and moment redistribution of RC continuous T-beams strengthened with FRP or steel bars by under repeated load.
3. It is preferable to strength the RC continuous beams at the sagging region only with the steel bars, because it help to increase the service and ultimate loads

REFERENCES

1. Jumaat MZ, Rahman MM, Rahman MA. (2011), Review on bonding techniques of CFRP in strengthening concrete structures. Int J Phys Sci; 6(15):3567–75.

2. El-Hacha R, Soudki K. (2013), Prestressed near-surface mounted fibre reinforced polymer reinforcement for concrete structures – a review. NRC Research Press. Can J Civil Eng.; 40:1127–39.
3. Y. Al-Salloum, S.E. El-Gamal, T. Almusallam, S. Alsayed, M. Aqel. (2013), Effect of harsh environmental conditions on the tensile properties of GFRP bars, Compos. B 45 (1) 835–844.
4. Parretti R, Nanni A. (2004), Strengthening of RC members using near-surface mounted FRP composites: design overview. Advances in Structural Engineering; 7(6). 469:483.
5. De Lorenzis L, Teng JG. (2007), Near-surface mounted FRP reinforcement: an emerging technique for strengthening structures. Composites: Part B; 38:119–43.
6. Al-Mahmoud F, Castel A, François R, and Tourneur C. (2010) , RC beams strengthened with NSM CFRP rods and modeling of peeling-off failure. Composite Structures 92 1920–1930.
7. Rahman SMH, Mahmoud K, El-Salakawy E. (2017), “Behavior of Glass Fiber–Reinforced Polymer Reinforced Concrete Continuous T-Beams”. J. Compos. Constr., 21(2):
8. Rahman SMH, Mahmoud K, El-Salakawy E (2017),” Moment redistribution in glass fiber reinforced polymer-reinforced concrete continuous beams subjected to unsymmetrical loading”. Engineering Structures 150. 562–572.
9. Carmo NFC, Lopes SMR. (2008), Available plastic rotation in continuous high-strength concrete beams. Can J Civil Eng; 35(10):1152–62.
10. Maghsoudia A. A. and Akbarzadeh H. Bengarb. (2011), “Acceptable lower bound of the ductility index and serviceability state of RC continuous beams strengthened with CFRP sheets”. Scientia Iranica, Transactions A: Civil Engineering Vol.18, No.1, pp. 36–44.
11. Mahmoud K, El-Salakawy E. (2014), Shear strength of GFRP-reinforced concrete continuous beams with minimum transverse reinforcement. ASCE, J Compos Constr; 18(1):04013018.
12. Mostofinejad D. (1997), Ductility and moment redistribution in continuous FRP reinforced concrete beams PhD thesis. Ottawa, Ontario, Canada: Department of Civil and Environmental Engineering, Carleton University.
13. Grace NF, Soliman AK, Abdel-Sayed G, (1998), Saleh KR. Behavior and ductility of simple and continuous FRP reinforced beams. ASCE, J Compos Constr; 2 (4):186–94.
14. Habeeb MN, Ashour AF. (2008), Flexural behavior of continuous GFRP reinforced concrete beams. ASCE, J Compos Constr; 12(2):115–24.
15. El-Mogy M, El-Ragaby A, El-Salakawy E. (2014), Flexural behavior of continuous FRP reinforced concrete beams. ASCE, J Compos Constr; 14(6):669–80.
16. Kara IF, Ashour AF. (2013), Moment redistribution in continuous FRP reinforced concrete beams. Constr Build Mater; 49:939–48.
17. Santos P, Laranja G, Franca PM, Correia JR. (2013), Ductility and moment redistribution capacity of multi-span t-section concrete beams reinforced with GFRP bars. Constr Build Mater; 49:949–61.
18. Mahmoud K, El-Salakawy E. (2016), Effect of transverse reinforcement ratio on the shear strength of GFRP-RC continuous beams. ASCE, J Compos Constr; 20 (1):04015023..
19. Rahman SMH, Mahmoud K, El-Salakawy E. (2016), Behavior of glass fiber-reinforced polymer reinforced concrete continuous T-Beams. ASCE, J Compos Constr.
20. ACI 318M-1^ξ, Building Code Requirements for Structural Concrete. An ACI Standard and Commentary, March (2015).
21. Egyptian code of practice for design and construction of concrete structures ECCS 203- (2017).
22. F. Al-Mahmoud, A. Castel, R. François, C. Tourneur. (2009), Strengthening of RC members with near-surface mounted CFRP rods, Compos. Struct. 91 (2) 138–147.
23. American Concrete Institute (ACI). (2015) “Guide for the Design and Construction of Concrete Reinforced with FRP Bars.” ACI 440.1R-15, Farmington Hills, Mich.